

## Effect of interlamellar interactions on shear induced multilamellar vesicle formation

Y. Kawabata, R. Bradbury, S. Kugizaki, K. Weigandt, Y. B. Melnichenko, K. Sadakane, N. L. Yamada, H. Endo, M. Nagao, and H. Seto

Citation: *The Journal of Chemical Physics* **147**, 034905 (2017); doi: 10.1063/1.4994563

View online: <http://dx.doi.org/10.1063/1.4994563>

View Table of Contents: <http://aip.scitation.org/toc/jcp/147/3>

Published by the [American Institute of Physics](#)

---

---



**COMPLETELY  
REDESIGNED!**

**PHYSICS  
TODAY**

*Physics Today* Buyer's Guide  
Search with a purpose.

# Effect of interlamellar interactions on shear induced multilamellar vesicle formation

Y. Kawabata,<sup>1,a)</sup> R. Bradbury,<sup>2,3</sup> S. Kugizaki,<sup>1</sup> K. Weigandt,<sup>3</sup> Y. B. Melnichenko,<sup>4,b)</sup> K. Sadakane,<sup>5</sup> N. L. Yamada,<sup>6</sup> H. Endo,<sup>6</sup> M. Nagao,<sup>2,3,c)</sup> and H. Seto<sup>6,d)</sup>

<sup>1</sup>Department of Chemistry, Tokyo Metropolitan University, Hachioji, Tokyo 192-0397, Japan

<sup>2</sup>Center for Exploration of Energy and Matter, Department of Physics, Indiana University, Bloomington, Indiana 47408, USA

<sup>3</sup>NIST Center for Neutron Research, National Institute of Standards and Technology, Gaithersburg, Maryland 20899-6102, USA

<sup>4</sup>Biology and Soft Matter Division, Oak Ridge National Laboratory, Oak Ridge, Tennessee 37831-6393, USA

<sup>5</sup>Faculty of Life and Medical Sciences, Doshisha University, Kyotanabe, Kyoto 610-0321, Japan

<sup>6</sup>Institute of Materials Structure Science, High Energy Accelerator Research Organization, Tokai 319-1106, Japan

(Received 24 March 2017; accepted 5 July 2017; published online 21 July 2017)

Shear-induced multilamellar vesicle (MLV) formation has been studied by coupling the small-angle neutron scattering (SANS) technique with neutron spin echo (NSE) spectroscopy. A 10% mass fraction of the nonionic surfactant pentaethylene glycol dodecyl ether (C<sub>12</sub>E<sub>5</sub>) in water was selected as a model system for studying weak inter-lamellar interactions. These interactions are controlled either by adding an anionic surfactant, sodium dodecyl sulfate, or an antagonistic salt, rubidium tetraphenylborate. Increasing the charge density in the bilayer induces an enhanced ordering of the lamellar structure. The charge density dependence of the membrane bending modulus was determined by NSE and showed an increasing trend with charge. This behavior is well explained by a classical theoretical model. By considering the Caillé parameters calculated from the SANS data, the layer compressibility modulus  $\bar{B}$  is estimated and the nature of the dominant inter-lamellar interaction is determined. Shear flow induces MLV formation around a shear rate of 10 s<sup>-1</sup>, when a small amount of charge is included in the membrane. The flow-induced layer undulations are in-phase between neighboring layers when the inter-lamellar interaction is sufficiently strong. Under these conditions, MLV formation can occur without significantly changing the inter-lamellar spacing. On the other hand, in the case of weak inter-lamellar interactions, the flow-induced undulations are not in-phase, and greater steric repulsion leads to an increase in the inter-lamellar spacing with shear rate. In this case, MLV formation occurs as the amplitude of the undulations gets larger and the steric interaction leads to in-phase undulations between neighboring membranes. *Published by AIP Publishing.* [<http://dx.doi.org/10.1063/1.4994563>]

## I. INTRODUCTION

Lytotropic liquid crystals comprising amphiphilic molecules in hexagonal, lamellar, and cubic geometries have attracted a lot of interest in various fields across physics, chemistry, and biology. It is known that these ordered structures can transform with a change of external stimuli such as temperature, pressure, or concentration. Shear flow is also known to lead to structural transformation in these systems, and many studies about the shear effects on lyotropic phases have been reported.

For more than 20 years, many researchers have investigated shear effects on the lamellar phase by means of microscopy, nuclear magnetic resonance, and small angle

light/X-ray/neutron scattering. Generally, the lamellar bilayer stacking is aligned with the shear flow. Alternatively, Roux *et al.* have reported that with increasing shear rate, the aligned bilayers stack periodically to form multi-lamellar vesicles (MLVs), or “onions,” which fill all the space of a solution without excess water.<sup>1,2</sup> Interestingly, MLV formation in these systems is associated with shear-thickening rheological behavior. Due to these interesting properties, the shear-induced structural and rheological transitions in nonionic and ionic surfactant solutions have been frequently studied in recent years.<sup>1–32</sup>

One successful model that explains the MLV formation is the “buckling” model proposed by Zilman and Granek,<sup>33</sup> in which the bending and buckling of the aligned bilayer stacks occur at a critical shear rate and planar bilayer stacks transform to MLVs with a polyhedral shape. The critical shear rate or buckling wavelength are expressed in the model using the bending rigidity of bilayers  $\kappa$  and the compressibility modulus  $\bar{B}$ .<sup>33–35</sup> Therefore,  $\kappa$  and inter-lamellar interactions expressed through  $\bar{B}$  are key controlling parameters for MLV

<sup>a)</sup>Electronic mail: youheik@tmu.ac.jp

<sup>b)</sup>Y. B. Melnichenko is deceased as of 18 March 2016. He contributed this paper as an expert on small-angle neutron scattering.

<sup>c)</sup>Electronic mail: mnagao@indiana.edu

<sup>d)</sup>Electronic mail: hideki.seto@kek.jp

formation.<sup>33–35</sup> A comparison between a theoretical model and an experimental result was reported for the elastic properties of the membranes by Zhou and colleagues, but quantitative agreement was not observed.<sup>19</sup> The relation between the elastic moduli and MLV formation has not been clarified experimentally, i.e., the elastic moduli have not been estimated systematically using experimental techniques in lamellar phase solutions where the onion phase is induced by shear flow.

In this article, we have focused on MLV formation under shear flow in dilute lamellar phase solutions of  $C_{12}E_5$ /water with varying inter-lamellar interactions. The interactions were controlled by adding charged molecules to the nonionic membranes. The effect of charge in nonionic surfactant membranes on the onion formation and rheological properties has been investigated previously by other researchers.<sup>19,36,37</sup> They claimed that the increase of the electrostatic repulsion results in a stiffening of the membrane that suppresses layer undulations. Here, we determined the dependence of  $\kappa$  and  $\bar{B}$  on the charge density by means of small-angle neutron scattering (SANS) and neutron spin echo (NSE) and discuss the relation between the elastic moduli and the MLVs formation, which was investigated with simultaneous SANS and rheology measurements (rheo-SANS).

## II. EXPERIMENTAL

Pentaethylene glycol dodecyl ether,  $C_{12}E_5$ , was used as the nonionic surfactant and the main component of the bilayer dispersed in  $D_2O$ . Here,  $D_2O$  was employed to enhance the neutron scattering contrast between the bilayer and the solvent. Charge density in the non-charged bilayers was controlled by the addition of an anionic surfactant, sodium dodecyl sulfate (SDS). To check the generality of adding a charged agent, the addition of an antagonistic salt, rubidium tetraphenylborate ( $RbBPh_4$ ), was also investigated. Note that the hydrophilic cations and hydrophobic anions of an antagonistic salt are preferentially dissolved in water and oil regions, respectively, and a cation and anion pair acts like a surfactant molecule such that the interfacial tension between water and oil regions is decreased.<sup>38–44</sup> Thus, it is expected that hydrophobic anions are incorporated in the hydrophobic part of non-charged bilayers, while the hydrophilic cations remain in the water region, and that the antagonistic salt plays a similar role to the anionic surfactant.  $C_{12}E_5$  (purity > 98%) was purchased from Nikko Chemicals,  $RbBPh_4$  (purity 95%) from SIGMA Aldrich, SDS (purity better than 97%) from Tokyo Chemical Industry, Co., and  $D_2O$  (99.9% D) from Cambridge Isotope Laboratory, Inc., respectively.

The molar ratio between charged species and  $C_{12}E_5$ ,  $C$ , was varied between  $0.001 \leq C \leq 0.04$ , in order to control the surface charge density and the inter-layer interaction. The mass fraction of the nonionic surfactant and charged species was kept constant at 0.1. Non-charged  $C_{12}E_5$  molecules in water has been one of the classical microemulsion systems and, as such, the phase behavior is well-known.<sup>45</sup> When  $C_{12}E_5$  with a mass fraction of 10% is dissolved in water, a micellar phase ( $L_1$ ) appears at low temperature, while a lamellar phase ( $L_\alpha$ ) exists around 60 °C. A further increase in temperature results in the formation of a sponge phase ( $L_3$ ), which appears

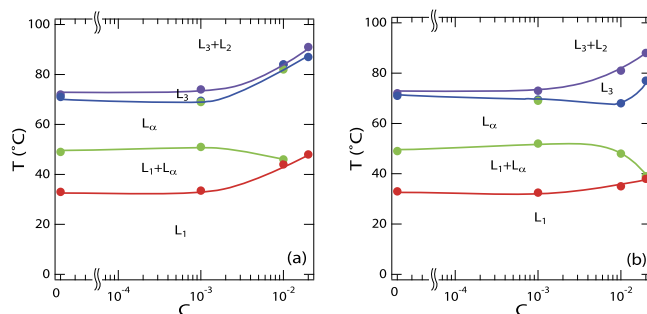


FIG. 1. Phase diagram of either (a) SDS or (b)  $RbBPh_4$  containing  $C_{12}E_5$ / $D_2O$  solutions with varying the molar ratio of the charged species,  $C$ . With increasing  $C$ , the lamellar  $L_\alpha$  phase was enlarged, while the two regions of phase separation between  $L_\alpha$  and micellar phase  $L_1$  were shrunk.

only across a very narrow temperature range. The addition of a charged species changes the phase behavior as shown in Fig. 1. Figure 1(a) shows the phase diagram with added SDS. If more SDS is added, the low temperature phase separation region is reduced in size, while the size of the sponge region does not change significantly. These characteristics are consistent with the phase behavior known in the literature.<sup>46</sup> The mixture with  $RbBPh_4$  was found to have a very similar phase diagram, as shown in Fig. 1(b). This suggests that an antagonistic salt plays the same role as a cationic surfactant in modifying the charge of the non-ionic surfactant bilayers.

SANS experiments were conducted on the CG2 General Purpose SANS at the Oak Ridge National Laboratory (ORNL), and the NG7-30 m SANS instrument at the National Institute of Standards and Technology (NIST).<sup>47</sup> The measured momentum transfer,  $q$ , ranged from  $0.04 \text{ nm}^{-1}$  to  $5 \text{ nm}^{-1}$ . These instruments were used to investigate charge effects on the structure at steady state. In order to measure the SANS profile under shear flow, a rheo-SANS setup<sup>48</sup> was used at the NGB-10 m SANS at the NIST. Since a wide phase separation region exists below the  $L_\alpha$  phase, we could not reach a stable  $L_\alpha$  phase by increasing the temperature from the  $L_1$  phase. Instead, we loaded the sample in the  $L_3$  phase, which appears at a higher temperature than the  $L_\alpha$  phase, then cooled the sample temperature down to the target temperature of  $(58 \pm 1.5)^\circ\text{C}$ . We confirmed that the sample appearance did not change in this process by visual inspection, which supports the formation of  $L_\alpha$  at  $T = 58^\circ\text{C}$ . Using this approach, we could reach the  $L_\alpha$  phase in the rheometer and avoid phase separation during sample loading. The measured  $q$  range was from  $0.1 \text{ nm}^{-1}$  to  $1 \text{ nm}^{-1}$  for the rheo-SANS setup. The data reduction procedures at each facility were used to reduce the SANS data,<sup>49</sup> and some of the data analysis was performed using Sas View.<sup>50</sup>

NSE experiments were performed using the NGA-NSE spectrometer at the NIST.<sup>51</sup> NSE measures the bilayer bending elastic constants, and therefore charge effects on the bending modulus,  $\kappa$ , were extracted. The incident neutron wavelengths were  $8 \text{ \AA}$  and  $11 \text{ \AA}$  so that we reach the maximum Fourier time of 40 ns and 100 ns, respectively. The measured  $q$  range was from  $0.4 \text{ nm}^{-1}$  to  $1.7 \text{ nm}^{-1}$ . The temperature was controlled in demountable titanium cells with quartz windows using a water circulating bath system. The sample temperature was set at  $58^\circ\text{C}$  within the deviation of  $\pm 1.5^\circ\text{C}$ . The measured data

were corrected against the standard elastic scattering sample and the background using the DAVE software.<sup>52</sup>

### III. RESULTS AND DISCUSSION

#### A. Steady state structure

Figure 2(a) presents the charge density dependence of SANS profiles as a function of added SDS. Although a binary mixture of a mass fraction of 10% C<sub>12</sub>E<sub>5</sub> in D<sub>2</sub>O is known to form lamellar structures at  $T = 58^\circ\text{C}$ , the present SANS pattern does not show any significant peaks from the aligned lamellar layers. The form factor region is explained well using the model function proposed by Nallet *et al.*<sup>53</sup> This model, combined with visual inspection, suggests that this pattern originates from the randomly oriented lamellar structures. When a small amount of SDS is added to the nonionic bilayer, 1 SDS molecule to 1000 C<sub>12</sub>E<sub>5</sub> molecules already has a significant effect on the interaction between the layers. A broad peak appears around  $q = 0.2 \text{ nm}^{-1}$ , which comes from the interlayer spacing unit of the lamellar structure. This peak becomes sharper as the SDS content is increased up to the maximum charge concentration tested ( $C = 0.04$ ). The position of the first peak seems slightly modulated with increasing SDS concentration but the change is not significant.

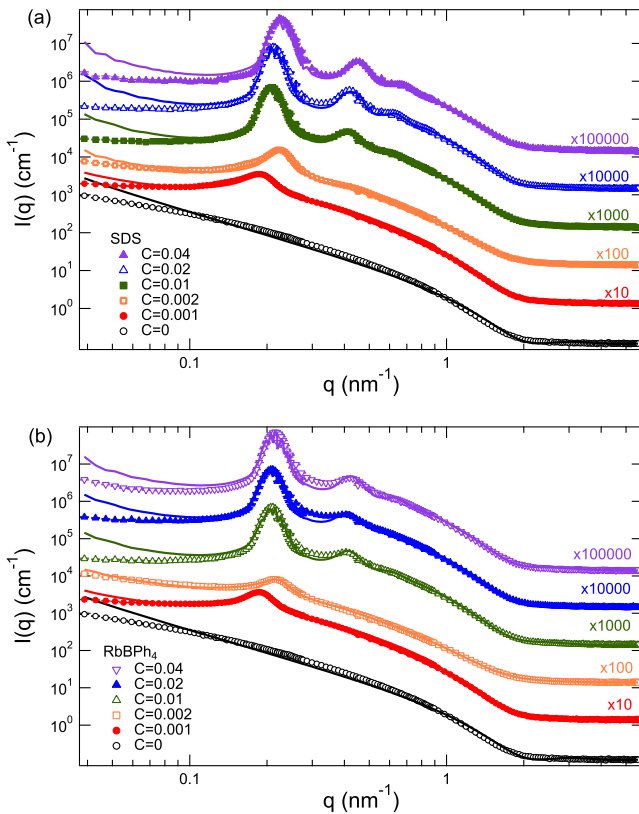


FIG. 2. SANS patterns observed when increasing the amount of (a) SDS and (b) RbBPh<sub>4</sub> in C<sub>12</sub>E<sub>5</sub> bilayers in D<sub>2</sub>O at  $T = 58^\circ\text{C}$ . Legend indicates the molar ratio,  $C$ , of (a) SDS and (b) RbBPh<sub>4</sub> to C<sub>12</sub>E<sub>5</sub>. Data set is shifted by the indicated multiplication factor except for pure components, which is shown in absolute scale unit of  $\text{cm}^{-1}$ . Solid lines indicate fit results according to the model proposed by Nallet *et al.*<sup>53</sup> Error bars represent  $\pm 1$  standard deviation throughout the paper.

Figure 2(b) displays the SANS profiles for the case where RbBPh<sub>4</sub> is added to the system. It is clear that the concentration dependence of the SANS profile is very similar to that for SDS. This indicates that the antagonistic salts are distributed in the C<sub>12</sub>E<sub>5</sub> bilayers and contribute to the interlayer interaction to a similar degree compared to the SDS. Similar trends for the scattering peak growth and peak location were observed for various other antagonistic salt conditions (data not shown). Thus, it has been confirmed that the addition of the antagonistic salt modifies the inter-bilayer interaction in the same manner as the SDS. Note that a hydrophilic salt, such as NaCl, did not alter the scattering pattern of the pure C<sub>12</sub>E<sub>5</sub> membranes at this low concentration, since the hydrophilic salt dissolving in the water phase does not have a significant charge contribution to the interlayer interaction.

As shown in Fig. 2, the scattering theory to describe the lyotropic lamellar phase of surfactant solutions<sup>53</sup> explains our scattering results quite well except for deviations in the lowest  $q$  regions. These deviations suggest a larger scale structural inhomogeneity that may perturb the scattering intensity. Based on the model fit that accounts for the instrumental resolution smearing, we can deduce the mean repeat distance of the lamellar,  $d$ , the average thickness of the lamellar,  $\delta$ , and the Caillé parameter,  $\eta_{cp}$ , which is related to the membrane elastic constants. Figure 3 shows the charge density dependence of these parameters. This result indicates that  $\delta$  is almost constant when charged species are incorporated into the nonionic surfactant bilayers, while  $d$  may get smaller at low concentration and stays almost constant at higher charge conditions. A similar trend of the change in  $d$  was reported by Bergmeier *et al.* for mixed nonionic and ionic surfactants tetradecyldimethylamine-oxide (TDMAO) and tetradecyltrimethylammonium bromide (TTABr) bilayers.<sup>6</sup> The Caillé parameter,  $\eta_{cp}$ , can be expressed as<sup>53,54</sup>

$$\eta_{cp} = \frac{q_p^2 k_B T}{8\pi \sqrt{\kappa \bar{B}} / \delta}, \quad (1)$$

where  $q_p$  denotes the position of the first sharp correlation peak between bilayers,  $k_B T$  is the thermal energy,  $\kappa$  is the bending modulus, and  $\bar{B}$  is the compressibility modulus. As demonstrated in Fig. 3(b),  $\eta_{cp}$  is strongly dependent on the amount of charge. In the next section we use NSE to determine the bending modulus of the membrane  $\kappa$  and will discuss the effect of charge on the structure and dynamics more in detail.

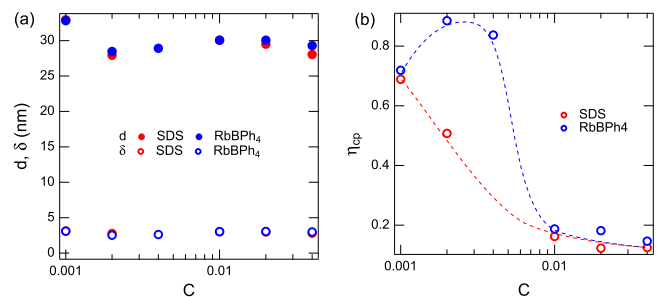


FIG. 3. Structural parameters determined by the fit of the SANS data. (a) Mean repeat distance  $d$  slightly decreases at low charge conditions, while overall values may be almost constant around 30 nm. The bilayer thickness  $\delta$  is almost constant at 3.0 nm for both charge cases. (b) Extracted Caillé parameter shows different behaviors at low charge concentration cases between anionic surfactant and antagonistic salt as highlighted by the dotted lines.

## B. Steady state equilibrium dynamics

NSE measures the intermediate scattering function,  $I(q, t)/I(q, 0)$ , as a function of  $q$  and Fourier time  $t$ , which is shown in Fig. 4 for the case of  $C_{12}E_5$  bilayers dispersed in  $D_2O$  at  $C = 0.001$  (RbBPh<sub>4</sub> has been added to the membrane). In the present system, without charged species, it has been established that the bilayer displays non-interacting undulation fluctuations, and a theoretical model to describe single membrane dynamics proposed by Zilman and Granek<sup>55</sup> explains the NSE result well.<sup>56</sup> The model is expressed as

$$\frac{I(q, t)}{I(q, 0)} = \exp \left[ - \left( 0.025 \gamma \sqrt{\frac{k_B T}{\kappa}} \frac{k_B T}{\eta_{D_2O}} q^3 t \right)^{2/3} \right], \quad (2)$$

where  $\gamma$  is a parameter close to unity originating from averaging the angle between the wavevector  $q$  and a vector normal to the bilayer, and  $\eta_{D_2O}$  is the viscosity of water. The present NSE result indicates that the Zilman-Granek model explains the data with the addition of a small amount of charged species quite well, even at the highest condition of  $C = 0.04$  as shown in the inset of Fig. 4. The excellent agreement with the scaling behavior of the Zilman-Granek model validates its use here. However, it is known that this model cannot estimate the absolute value of bending rigidity precisely because of the internal friction of the membranes. In order to solve this problem, we employed a simple treatment, whereby an effective solvent viscosity approximately three times of  $\eta_{D_2O}$  is used to estimate reasonable values of  $\kappa$  under the assumption of  $\gamma = 1$ .<sup>57,58</sup> This treatment contains an arbitrary factor that assumes an effective viscosity of between 2 and 4 times that of  $\eta_{D_2O}$ .<sup>58–60</sup> In a previous study, a factor of three worked well for a similar lamellar system with changing charge interactions.<sup>61</sup> Watson and Brown<sup>62</sup> presented a source of the discrepancy between the Zilman-Granek prediction and actual estimates of  $\kappa$  as an internal layer friction, originally considered by Seifert and Langer.<sup>63</sup>

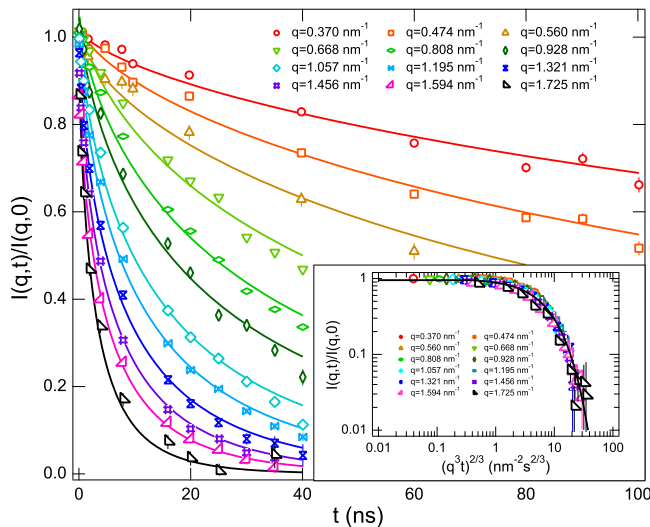


FIG. 4. Intermediate scattering function,  $I(q, t)/I(q, 0)$ , measured by NSE for  $C_{12}E_5$  bilayers in  $D_2O$  with the addition of RbBPh<sub>4</sub> at  $C = 0.001$ . Solid lines indicate the fit result according to the Zilman-Granek model.<sup>55</sup> Inset shows a scaling plot for the sample with RbBPh<sub>4</sub> at  $C = 0.04$  and the black line is the fit result to the scaling law.

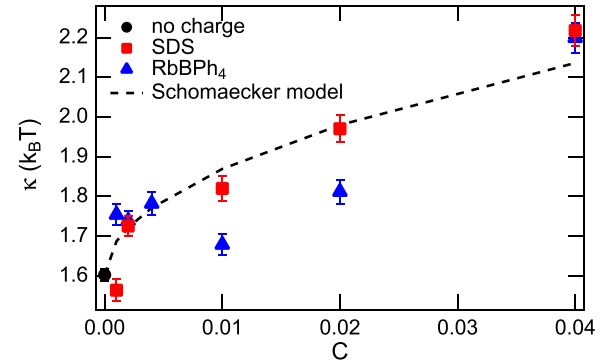


FIG. 5. Dependence of  $\kappa$  on the amount of charged species included in the system. Increase in  $\kappa$  with charge is consistent with the theoretical prediction.<sup>64</sup>

The estimated  $\kappa$  for pure  $C_{12}E_5$ , with SDS, and with RbBPh<sub>4</sub> are plotted in Fig. 5, which shows a monotonic increase of  $\kappa$  with  $C$ . The trend and magnitude of  $\kappa$  are comparable with the previous works on similar surfactant systems.<sup>61,64,65</sup> The contribution of charge to the bending modulus  $\kappa_c$  has been considered as an additive term to the geometric contribution  $\kappa_g$ .<sup>66–72</sup> The prediction used by Schomaecker and Strey<sup>64</sup> is based on the one proposed by Harden and colleagues<sup>69</sup> and is described as  $\kappa_c = 3k_B T / 4\pi \kappa_D^3 l_B l_{GC}^2$ , where  $\kappa_D^{-1}$  is the Debye length defined as  $\kappa_D^{-1} = \sqrt{\epsilon_r \epsilon_0 k_B T / 2ne^2}$ ,  $\epsilon_r$  is the dielectric constant of the solution,  $\epsilon_0$  is the vacuum permittivity,  $n$  is the charge number density, and  $e$  is the electric unit charge.  $l_B$  and  $l_{GC}$  are the Bjerrum length given by  $l_B = e^2 / 4\pi \epsilon_r \epsilon_0 k_B T$  and the Gouy-Chapman length given by  $l_{GC} = e / 2\pi l_B \sigma$  with  $\sigma$  the surface charge density, respectively. The dashed line in Fig. 5 indicates the result from the above calculation assuming the dissociation rate of 25% as measured in a  $C_{12}E_4$ /SDS/water/octane system,<sup>61</sup> which explains the experimental result well. Note that this tendency contradicts the experimental results given by Farago and Gradzielski,<sup>73</sup> the bending modulus of TDMAO monolayer does not change with the addition of TTABr. This discrepancy may originate from the differences between the samples and the geometry of the membranes.

Here, we combine both SANS and NSE data to understand charge effects on the steady state structure and dynamics in more detail. We observed a weak charge dependence of the interlamellar repeat distance,  $d$ , while an almost constant bilayer thickness,  $\delta$ , was calculated from the SANS data. The reduction of  $d$  with charge has been explained as the suppression of undulation fluctuations due to interlayer charge interactions.<sup>74</sup> The dilution law  $d = \delta / \phi$ , where  $\phi$  is the volume fraction of the bilayer, can be modified due to the membrane undulation and expressed as  $d = \delta(1 + \frac{\Delta A}{A}) / \phi$  where  $A$  is the area of the undulating bilayer projected on the normal plane and  $\Delta A + A$  is the average of the true area of the bilayer. In order to capture the charge effects on the bilayer undulations, de Vries proposed comparing the relative change in the dilution relation from an experiment and area change from theory as<sup>74</sup>

$$\left( \frac{d\phi}{\delta} \right)_2 - \left( \frac{d\phi}{\delta} \right)_1 = \left( \frac{\Delta A}{A} \right)_2 - \left( \frac{\Delta A}{A} \right)_1, \quad (3)$$

where  $(\Delta A/A)_n$  is given by

$$\left(\frac{\Delta A}{A}\right)_n = \frac{1}{4\pi\kappa_n} \int_0^{x_m} \frac{dx}{x} \left(1 + \frac{d_{w,n} f_e(x, \Lambda)}{\pi l_B \kappa_n x^4}\right)^{-1/2} \times \left(1 + \frac{d_{w,n} f_0(x, \Lambda)}{\pi l_B \kappa_n x^4}\right)^{-1/2}, \quad (4)$$

and  $x_m = q_m d_{w,n}/2$  with  $q_m = 2\pi/\delta$ ,  $d_{w,n}$  is the water layer thickness of species  $n$ ,  $\kappa_n$  is the experimentally determined bending modulus of species  $n$  from the NSE, and  $\Lambda = 2d_w/l_{GC}$ . The dimensionless functions  $f_e(x, \Lambda)$  and  $f_0(x, \Lambda)$  refer to the even and odd mode of the undulations, respectively, and the explicit expressions are given elsewhere.<sup>74</sup> Following the previous studies,<sup>61,74–76</sup> we calculated values for the difference in the bilayer area change at a given  $C$ ,  $(\Delta A/A)_2$  with respect to a reference value  $(\Delta A/A)_1$  and the results are shown in Fig. 6. The reference point was chosen to be  $C = 0.001$  for both SDS and RbBPh<sub>4</sub> cases. Calculations indicate a monotonic decrease of the area difference with increasing charge. This trend explains the experimental data points above  $C = 0.01$ . In between  $C = 0.001$  and  $0.01$ , the deviation between the experiment and calculation is unacceptably large. This suggests that in this range, the reduction of undulation fluctuations due to the increase in the bending rigidity of membranes cannot explain the change of the value of  $d$ . As was discussed in a similar system,<sup>61</sup> this difference may come from structural modifications, for example, vesicle formation as suggested previously.<sup>64,69</sup> Indeed, the SANS profile obtained in this region shown in Fig. 2 indicates increased intensity at low  $q$  region ( $C = 0.002$ ), which represents a longer range inhomogeneity in the system. It is noted that this tendency may be true for  $C = 0.001$  as well, but the increase in the low  $q$  intensity is not as large as the case for  $C = 0.002$  and we treat this in the same type of lamellar structure as the larger charge conditions.

After estimation of  $\kappa$  by NSE, the only unknown parameter in Eq. (1) is  $\bar{B}$  of the bilayer. The value of  $\bar{B}$  can thus be calculated, as shown in Fig. 7. This parameter indicates

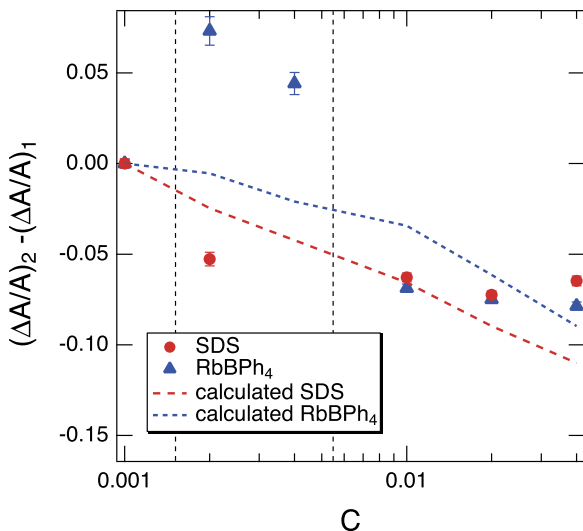


FIG. 6.  $C$  dependence of the difference in the change in area. The experimental data points are shown as the deviation from the dilution law  $[(\Delta A/A)_2 - (\Delta A/A)_1 = 0]$  corresponds to the dilution law and the dashed lines indicate the calculation of the area change using Eq. (4). The dashed vertical lines separate the regions that have some structural modification.

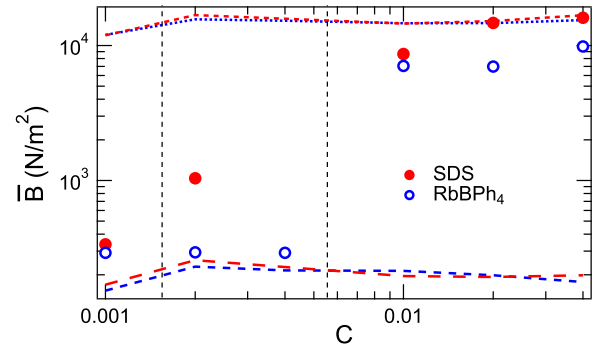


FIG. 7.  $C$  dependence of  $\bar{B}$  of the surfactant bilayers calculated from the combination between the Caillé parameter  $\eta_{cp}$  extracted from SANS and bending modulus  $\kappa$  from NSE. The dotted lines are the calculated values of  $\bar{B}$  assuming weakly screened electrostatic repulsions,  $\bar{B}_{el}$  [Eq. (5)], while the dashed lines are under the assumption of crumpled membranes with Helfrich's steric repulsion,  $\bar{B}_{str}$  [Eq. (6)]. The vertical dashed lines are the same as Fig. 6.

the layer compressibility modulus at constant chemical potential, which relates to the interactions between membranes.<sup>77</sup> In the case of weakly screened electrostatic repulsions as expected in the present system at high  $C$ , the exact form of the interaction potential is calculated from the one-dimensional Poisson-Boltzmann equation.<sup>78</sup> This form of  $\bar{B}$  is calculated as<sup>79,80</sup>

$$\bar{B}_{el} = \frac{\pi\kappa_B T d}{2l_B(d - \delta)^3} \quad (5)$$

and the calculated result is shown in Fig. 7 by the dotted lines. The calculated values of  $\bar{B}_{el}$  are on the order of  $10^4$  N/m<sup>2</sup> for all the charge concentrations. These values are at the low end of the scale for electrostatic repulsion and consistent with the values in the literature.<sup>81–83</sup> Therefore, in the large  $C$  regions, the membranes are primarily stabilized by the electrostatic repulsions. In the small  $C$  regions, the electrostatic interactions are not sufficient to stabilize the membranes, while steric repulsion due to thermal undulations of membranes<sup>84</sup> explains the experimental data much better. The value of  $\bar{B}$  for the undulating membranes is calculated as<sup>85</sup>

$$\bar{B}_{str} = \frac{9\pi^2(k_B T)^2 d}{64\kappa(d - \delta)^4}, \quad (6)$$

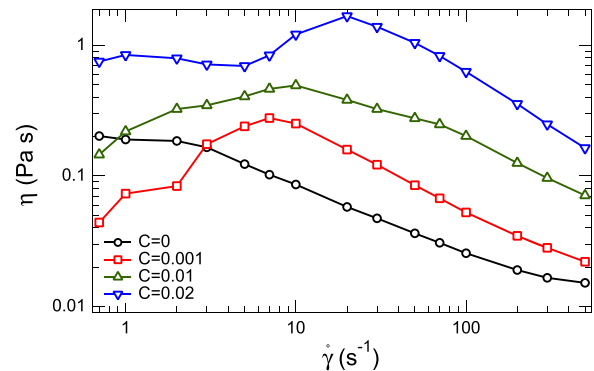


FIG. 8. Apparent viscosity in  $C_{12}E_5/SDS/D_2O$  systems under shear at  $C = 0, 0.001, 0.01,$  and  $0.02$ . Shear thickening is observed around  $\dot{\gamma}_c = 10$  s<sup>-1</sup>. The pure sample shows a slight shoulder around  $\dot{\gamma}_c = 3$  s<sup>-1</sup>, which can be a similar trend to the shear thickening seen in the charged systems.

and the result is shown by the dashed lines for each charge species (values on the order of  $10^2$  N/m<sup>2</sup>). These values are slightly smaller than the values reported by Tsapis *et al.*,<sup>86</sup> where their data were well explained by Helfrich's model with renormalized thickness.<sup>87</sup> Since their mean repeat distance is slightly smaller than ours, it is reasonable that we have smaller values of  $\bar{B}$ . As a matter of fact, Imai *et al.* reported even smaller  $\bar{B}$  than ours in the C<sub>12</sub>E<sub>5</sub>/water system with a larger mean repeat distance.<sup>59</sup> Therefore, we conclude that our membranes at low  $C$  are thermally fluctuating and the interaction is weak. It is noted here that the structural modifications at the intermediate regions of  $C$  may come from the fact that the interlayer electrostatic and steric interactions are competing with each other, which affects the stability of the structure.

### C. Structure under shear flow

Figure 8 represents the shear rate,  $\dot{\gamma}$ , dependence of the solution viscosity in a C<sub>12</sub>E<sub>5</sub>/SDS/water system with varying  $C$  from 0 to 0.02. The data show a clear trend of shear thickening and then thinning when a charged surfactant is added to the nonionic surfactant bilayers. The critical shear

rate  $\dot{\gamma}_c$  as the maximum of the viscosity shifts to higher  $\dot{\gamma}$  as the amount of SDS is increased. A similar trend was observed when the antagonistic salt RbBPh<sub>4</sub> is added to the C<sub>12</sub>E<sub>5</sub>/water system. Although the shear thickening behavior is clear with charged molecules present in the system, the non-charged C<sub>12</sub>E<sub>5</sub>/water system does not display a clear increase in the viscosity, though a slight shoulder is seen around  $\dot{\gamma}_c = 3$  s<sup>-1</sup>. The sharpness of the peak shape seems to vary with  $C$ , with a broader peak apparent for smaller  $C$ . A similar shear-thickening behavior and the peak shape variation were reported in TDMAO/TTABr/hexanol/water systems.<sup>5,6</sup> We suspect that the changes in the peak shape relate to the strength of the inter-lamellar interactions. When  $C$  is increased, the electrostatic repulsion is enhanced and the buckling occurs cooperatively. As a result, the viscosity peak becomes narrower and the apparent viscosity increases with increasing charge density.

Shear thickening behavior in the lamellar phase has been discussed in conjunction with the MLV formation under shear. In those cases, anisotropic scattering patterns change to isotropic ones due to vesicle formation.<sup>1,32,88</sup> Figure 9 shows a course of SANS patterns while changing  $\dot{\gamma}$ . Figures 9(a) and 9(b) are the two dimensional SANS patterns for radial

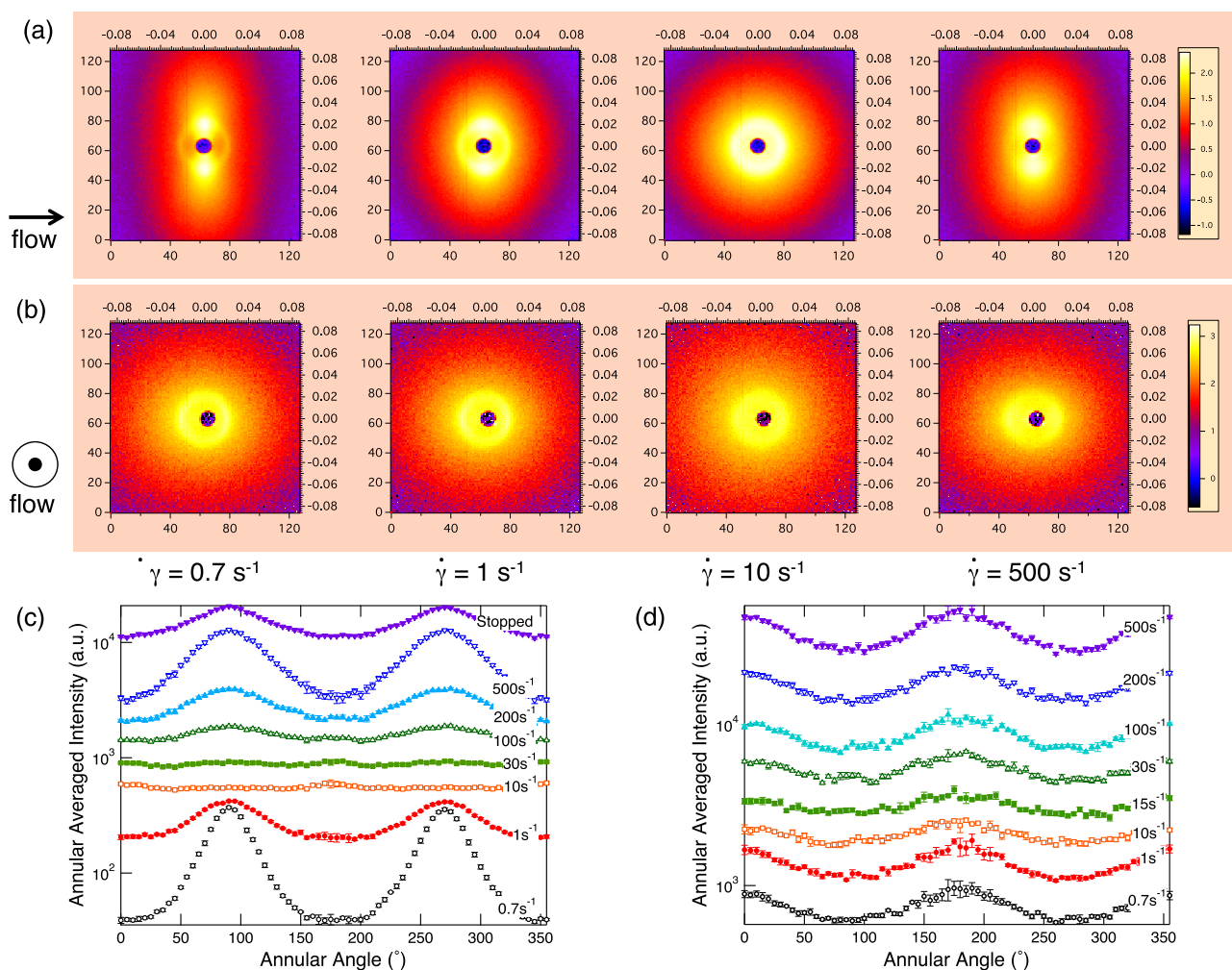


FIG. 9. [(a) and (b)] 2D SANS patterns from a RbBPh<sub>4</sub>/C<sub>12</sub>E<sub>5</sub>/D<sub>2</sub>O system at  $C = 0.001$  for a different shear rate  $\dot{\gamma}$  of (a) radial and (b) tangential configurations. The left and bottom axes indicate the pixel number of the neutron detector, and the top and right axes are the values of  $q$ . The color bar corresponds to the scattering intensity. The flow direction is shown at the left side of the 2D patterns. [(c) and (d)] Annular average of the 2D SANS pattern at  $q \approx 0.2$  nm<sup>-1</sup> for (c) radial and (d) tangential configurations.

and tangential configurations observed for a RbBPh<sub>4</sub>/C<sub>12</sub>E<sub>5</sub>/D<sub>2</sub>O system at  $C = 0.001$ . In the radial configuration [Fig. 9(a)], the planar lamellar structure is aligned in the direction parallel to the flow at low  $\dot{\gamma}$ , while more isotropic scattering is observed around  $\dot{\gamma} = 10 \text{ s}^{-1}$ , and eventually at  $\dot{\gamma} = 500 \text{ s}^{-1}$ , the lamellar is again aligned parallel to the flow direction. In the tangential direction [Fig. 9(b)], the  $\dot{\gamma}$  dependence is less pronounced. As  $\dot{\gamma}$  is increased, the scattering pattern becomes isotropic at  $\dot{\gamma} \approx 10 \text{ s}^{-1}$ , while an anisotropic scattering pattern is again observed at higher shear rates. The annular average at  $q \approx 0.2 \text{ nm}^{-1}$  where the lamellar scattering peak is observed is presented in Figs. 9(c) and 9(d) for radial and tangential configurations, respectively. Again, the above mentioned anisotropic to isotropic to anisotropic scattering patterns are evident with increasing  $\dot{\gamma}$ . The present rheo-SANS result indicates that isotropic scattering is observed where the rheology measurement shows shear thickening and this is typical of the planar lamellar to MLV transition. Once MLVs are formed, the space is filled with spherical MLVs and isotropic scattering dominates the scattering pattern.

We measured rheo-SANS for RbBPh<sub>4</sub>/C<sub>12</sub>E<sub>5</sub>/D<sub>2</sub>O and SDS/C<sub>12</sub>E<sub>5</sub>/D<sub>2</sub>O at different levels of charged species, and similar anisotropic to isotropic to anisotropic scattering patterns are observed as we increase  $\dot{\gamma}$  for all these conditions. This implies that the initial state without shear flow is always the planar lamellar structure even at the large  $C$  conditions, and the data confirm that the shear thickening originates from the MLV formation. The critical shear rate showing the maximum viscosity increases with increasing charge amount in the bilayer, which indicates that MLV formation becomes less likely with increasing charge. Since the bending modulus measured by NSE increases with increasing charge content, buckling of the bilayers becomes less preferable and that reduces the likelihood of MLV formation. In the previous studies with TDMAO and TTABr membranes,<sup>5,6</sup> an opposite trend, where the critical shear rate decreases with increasing membrane charge density, was observed. These systems show vesicle formation without shear in the high charge density cases, and they speculated that the incorporation of charge in the membranes induces a reduction of the Gaussian modulus,  $\bar{\kappa}$ . A similar behavior, where the critical shear rate decreases with increasing charge, was also observed in a different surfactant system.<sup>19</sup> This system also forms a vesicle structure at high charge, in the absence of shear; however, in this case, the critical shear rate did increase slightly with charge at a lower concentration. This suggests that the system we present in this work is most similar to the low charge conditions in this other study.

In order to verify how the strength of the interlayer interaction affects the behavior, we calculated the  $\dot{\gamma}$  dependence of the mean repeat distance  $d$ . Figure 10 presents the result in the two extreme interaction cases for  $C = 0.001$  and  $0.02$  through two different flow directions in SDS/C<sub>12</sub>E<sub>5</sub>/D<sub>2</sub>O. The top panel is from a vertical slice from scattering through the tangential direction (shear gradient direction), the middle is from a vertical slice from scattering through the radial direction (shear neutral direction), and the bottom panel shows the result from a horizontal slice from scattering through the radial direction (shear flow direction), respectively. Above  $\dot{\gamma} = 1 \text{ s}^{-1}$

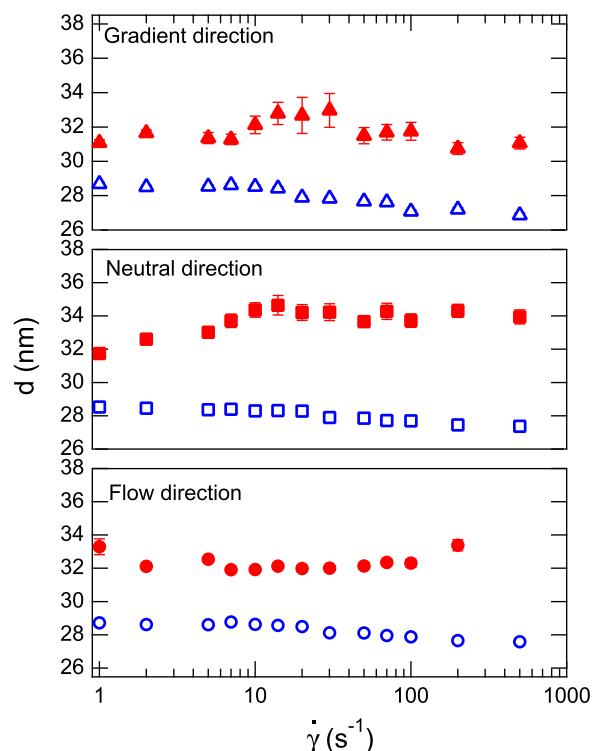


FIG. 10.  $\dot{\gamma}$  dependence of the mean repeat distance of the lamellar,  $d$ , for different observation directions. The flow and neutral directions correspond to the horizontal (circles) and vertical (squares) axes in the radial direction in the sample geometry, while the gradient direction is the horizontal (up-pointing triangles) axis in the tangential direction. Full symbols show the data from  $C = 0.001$  and open symbols from  $C = 0.02$  for the charge species as SDS.

for the  $C = 0.02$  sample, the data show almost the same trend as the data in the literature.<sup>36</sup> In the larger interlayer interaction case, the value of  $d$  stays almost constant at  $\dot{\gamma} \leq 20 \text{ s}^{-1}$  where the viscosity almost reaches a maximum, and then decreases with increasing  $\dot{\gamma}$ .

On the other hand, in the weaker interaction case at  $C = 0.001$ , we see slightly different behavior. Both in the neutral and gradient directions, the value of  $d$  increases with  $\dot{\gamma}$  at  $\dot{\gamma} \leq 10 \text{ s}^{-1}$ , while the flow direction shows an almost constant value of  $d$ . As seen in Fig. 8, the solution viscosity increases toward  $\dot{\gamma} \approx 10 \text{ s}^{-1}$ , where MLV formation is expected. Furthermore, in the two-dimensional SANS pattern, we observed isotropic scattering patterns at  $7 \text{ s}^{-1} \leq \dot{\gamma} \leq 100 \text{ s}^{-1}$ . Therefore, this trend of increasing  $d$  toward MLV formation is thought to be a signature of structural changes necessary for MLV formation. The value of  $d$  in the steady state, i.e.,  $\dot{\gamma} = 0$ , is observed to be  $d = 33 \text{ nm}$ , and the value of  $d$  was almost constant at the low shear rates for  $\dot{\gamma} < 1 \text{ s}^{-1}$  ( $d \approx 32 \text{ nm}$ ). Increasing the  $d$ -spacing is thus induced by the increased undulations due to the flow. This corresponds to the increase of the buckling instability, suggested theoretically<sup>33</sup> and confirmed experimentally,<sup>32</sup> leading to onion formation. As a matter of fact, if we calculate the change of the excess area due to the change in the undulation using de Vries theory [Eq. (3)],<sup>74</sup> we see about a  $1 k_B T$  drop of the bending rigidity from  $\dot{\gamma} = 1 \text{ s}^{-1}$  to  $\dot{\gamma} = 10 \text{ s}^{-1}$ . This kind of reduction is seen in both the flow and gradient directions and indicates increased undulations in these directions. We believe the present result provides further evidence

that the buckling instability induces MLV formation, and that, even in the weak interlayer interaction cases, the mechanism of the MLV formation is through the buckling.

In the strong inter-lamellar interaction cases, the undulations are more or less in-phase, and the shear flow induces an increase of the in-phase undulation fluctuations, which leads to MLV formation through buckling instability. For the weaker interaction case, the flow-induced undulations are out-of-phase between neighboring membranes. The flow-induced undulations increase the steric repulsion between membranes, which is responsible for the increase in  $d$ . As the steric interactions get larger, the undulations become more in-phase and eventually overcome the threshold for MLV formation. When the inter-membrane interactions are even smaller, like the case of no-charge membranes in the present experiment, shear flow induces further undulations, where neighboring membranes are out-of-phase. As the shear rate increases, the amplitude of the undulations gets larger, while the steric repulsion between the membranes is not strong enough to buckle them together. As such, the system still prefers to transform to vesicular structures. In this case, unilamellar vesicles instead of MLVs would be induced as was suggested by a theoretical study.<sup>31</sup> The shoulder seen in the viscosity data (Fig. 8) may come from this type of structural change.

Before closing the discussion, we should note that there are some remaining issues to be solved. First, is the observation of a lower viscosity at low shear rate for  $C = 0.001$  compared with that at  $C = 0$ . We would expect that larger inter-lamellar interactions induce a higher apparent viscosity, which is confirmed at high shear rate, but not at low shear rate (see Fig. 8). The second issue is the different SDS dependence of the Caillé parameters of the samples with SDS and RbBPh<sub>4</sub> when a small amount of charge is added (see Fig. 3). This may reflect the different charge distribution within the membranes. The SANS profiles at  $C = 0.002$  in Fig. 2 show a more asymmetric shape of the scattering peak for the sample with SDS. This suggests some kind of inhomogeneity in the lamellar membranes that is more pronounced in the SDS containing bilayers. Since these issues are not essential for the present study and further systematic experiments are necessary, we leave them as future problems.

#### IV. CONCLUSION

In the present paper, a combination of conventional SANS, rheo-SANS, and NSE has been used to demonstrate shear-induced multilamellar vesicle (MLV) formation in a mass fraction of 10% C<sub>12</sub>E<sub>5</sub> aqueous solution. By controlling the inter-lamellar interactions through the addition of anionic surfactant SDS or antagonistic salt RbBPh<sub>4</sub>, the strength of inter-lamellar interactions and membrane elastic properties is shown to be interconnected with the mechanisms of MLV formation. The rheological behavior of the system shown in Fig. 8 was explained thus: The increase in the viscosity  $\eta$  with increasing the amount of charge,  $C$ , is due to the increase in the inter-lamellar repulsive interactions. This was evidenced by the conventional SANS experiment that clearly showed the inter-lamellar correlation peak to be sharper at the highest charge concentrations. Furthermore, through the use of NSE

to determine the bending modulus of the membrane,  $\kappa$ , the interaction strength between membranes was verified by calculating the layer compressibility modulus  $B$ . Shear thickening occurs due to MLV formation, which was less preferable at higher  $C$  (need higher shear to form MLVs), due to a larger  $\kappa$ . In the case when inter-lamellar interactions are sufficiently strong, the inter-lamellar spacing,  $d$ , did not change toward MLV formation. This indicates that the buckling instability induced by the flow shifted the membrane undulations closer to being in-phase. Once the MLVs were formed,  $d$  got smaller with increasing shear rate due to the water being squeezed out of the MLVs. When charge interactions are weak, however, an increase in  $d$  was observed in the flow and gradient directions toward the formation of MLVs, which indicated an increase of undulation fluctuations due to the flow. Since  $d$  stays constant if the membrane undulations are in-phase, this supports the existence of out-of-phase behavior, and an increase in the amplitude of the undulations increases the steric repulsion between the membranes. When the repulsion exceeds a certain level, the undulations become more in-phase and MLVs are formed, though if the repulsion stays weaker, then unilamellar vesicles may be formed under shear. The present result confirms that the buckling instability is the primary mechanism to form MLVs even in the weak interaction cases.

As a final remark, we clarify that the interplay between the inter-lamellar interactions and membrane elastic properties governs the buckling instability in the MLV formation process; the bending elasticity plays a major role in the case of weak inter-lamellar interactions, while the interactions override the key role when charge in the membrane is increased as well as inter-bilayer distance is decreased. This evidence could be indispensable information in understanding the mechanism of the shear induced MLV formation.

#### ACKNOWLEDGMENTS

The authors acknowledge Professor Tadashi Kato for his support to the experiments and discussion. Experimental support by Dr. Lilin He at ORNL and Professor Paul Sokol and Dr. Narayan Das at Indiana U. is acknowledged. This work was supported by a Grant-in-aid for Scientific Research A (Grant No. 23244088) from the Ministry of Education, Culture, Sports, Science and Technology (MEXT) of Japan. R.B. and M.N. acknowledge funding support of Cooperative Agreement No. 70NANB15H259 from NIST, U.S. Department of Commerce. The SANS experiments at ORNL were performed under the approval of the steering committee of US-Japan Collaborative Program on Neutron Scattering. Access to the NGA-NSE was provided by the Center for High Resolution Neutron Scattering, a partnership between the National Institute of Standards and Technology and the National Science Foundation under Agreement No. DMR-1508249. Portions of this work benefited from and provided support to the NIST nSoft consortium ([www.nist.gov/nsoft](http://www.nist.gov/nsoft)), including the use of the 10 m Small Angle Neutron Scattering instrument at the NCNR. Travel expenses of Y.K. and S.K. for the SANS and NSE experiments at the NIST were supported by General User Program for Neutron Scattering Experiments, Institute for Solid State Physics, The University of Tokyo, and the overseas

dispatching program for graduate students, Tokyo Metropolitan University, respectively. Certain commercial materials are identified in this paper to foster understanding. Such identification does not imply recommendation or endorsement by the National Institute of Standards and Technology (NIST) nor does it imply that the materials identified are necessarily the best available for the purpose.

- <sup>1</sup>O. Diat, D. Roux, and F. Nallet, "Effect of shear on a lyotropic lamellar phase," *J. Phys. II* **3**, 1427–1452 (1993).
- <sup>2</sup>D. Roux, F. Nallet, and O. Diat, "Rheology of lyotropic lamellar phases," *Europhys. Lett.* **24**, 53–58 (1993).
- <sup>3</sup>O. Diat, D. Roux, and F. Nallet, "'Layering' effect in a sheared lyotropic lamellar phase," *Phys. Rev. E* **51**, 3296–3299 (1995).
- <sup>4</sup>R. Weigel, J. W. Lauger, W. Richtering, and P. Linder, "Anisotropic small angle light and neutron scattering from a lyotropic lamellar phase under shear," *J. Phys. II* **6**, 529–542 (1996).
- <sup>5</sup>M. Bergmeier, M. Gradzielski, H. Hoffmann, and K. Mortensen, "Behavior of a charged vesicle system under the influence of a shear gradient: A microstructural study," *J. Phys. Chem. B* **102**, 2837–2840 (1998).
- <sup>6</sup>M. Bergmeier, M. Gradzielski, H. Hoffmann, and K. Mortensen, "Behavior of ionically charged lamellar systems under the influence of a shear field," *J. Phys. Chem. B* **103**, 1605–1617 (1999).
- <sup>7</sup>S. Muller, C. Borschig, W. Gronski, C. Schmidt, and D. Roux, "Shear-induced states of orientation of the lamellar phase of C<sub>12</sub>E<sub>4</sub>/water," *Langmuir* **15**, 7558–7564 (1999).
- <sup>8</sup>T. D. Le, U. Olsson, and K. Mortensen, "Topological transformation of a surfactant bilayer," *Phys. B (Amsterdam, Neth.)* **276-278**, 379–380 (2000).
- <sup>9</sup>J. I. Escalante, M. Gradzielski, H. Hoffmann, and K. Mortensen, "Shear-induced transition of originally undisturbed lamellar phase to vesicle phase," *Langmuir* **16**, 8653–8663 (2000).
- <sup>10</sup>J. Zipfel, F. Nettesheim, P. Lindner, T. D. Le, U. Olsson, and W. Richtering, "Cylindrical intermediates in a shear-induced lamellar-to-vesicle transition," *Europhys. Lett.* **53**, 335–341 (2001).
- <sup>11</sup>W. Richtering, "Rheology and induced structures in surfactant solutions," *Curr. Opin. Colloid Interface Sci.* **6**, 446–450 (2001).
- <sup>12</sup>K. Mortensen, "Structural studies of lamellar surfactant systems under shear," *Curr. Opin. Colloid Interface Sci.* **6**, 140–145 (2001).
- <sup>13</sup>M. G. Berni, C. J. Lawrence, and D. Machin, "A review of the rheology of the lamellar phase in surfactant system," *Adv. Colloid Interface Sci.* **98**, 217–243 (2002).
- <sup>14</sup>S. W. Marlow and P. D. Olmsted, "The effect of shear flow on the Helfrich interaction in lyotropic lamellar systems," *Eur. Phys. J. E* **8**, 485–497 (2002).
- <sup>15</sup>C. Oliviero, L. Coppola, R. Gianferri, I. Nicotera, and U. Olsson, "Dynamic phase diagram and onion formation in the system," *Colloids Surf., A* **228**, 85–90 (2003).
- <sup>16</sup>B. Medronho, S. Fujii, W. Richtering, M. G. Miguel, and U. Olsson, "Reversible size of shear-induced multi-lamellar vesicles," *Colloid Polym. Sci.* **284**, 317–321 (2005).
- <sup>17</sup>S. Fujii and W. Richtering, "Size and viscoelasticity of spatially confined multilamellar vesicles," *Eur. Phys. J. E* **19**, 139–148 (2006).
- <sup>18</sup>B. Medronho, M. G. Miguel, and U. Olsson, "Viscoelasticity of a nonionic lamellar phase," *Langmuir* **23**, 5270–5274 (2007).
- <sup>19</sup>A. Zou, H. Hoffmann, N. Freberger, and O. Glatter, "Influence of ionic charges on the bilayers of lamellar phases," *Langmuir* **23**, 2977–2984 (2007).
- <sup>20</sup>B. Medronho, S. Shafaei, R. Szopko, M. G. Miguel, and U. Olsson, "Shear-induced transitions between a planar lamellar langmuir phase and multi-lamellar vesicles: Continuous versus discontinuous transition," *Langmuir* **24**, 6480–6486 (2008).
- <sup>21</sup>B. Medronho, M. Rodrigues, R. Szopko, M. G. Miguel, U. Olsson, and C. Schmidt, "Shear-induced defect formation in a nonionic lamellar phase," *Langmuir* **26**, 11304–11313 (2010).
- <sup>22</sup>Y. Kosaka, M. Ito, Y. Kawabata, and T. Kato, "Lamellar-to-onion transition with increasing temperature under shear flow in a nonionic surfactant/water system," *Langmuir* **26**, 3835–3842 (2010).
- <sup>23</sup>Y. Suganuma, M. Imai, T. Kato, U. Olsson, and T. Takahashi, "Order-disorder transition of nonionic onions under shear flow," *Langmuir* **26**, 7988–7995 (2010).
- <sup>24</sup>M. Ito, Y. Kosaka, Y. Kawabata, and T. Kato, "Transition processes from the lamellar to the onion state with increasing temperature under shear flow in a nonionic surfactant/water system studied by rheo-SAXS," *Langmuir* **27**, 7400–7409 (2011).
- <sup>25</sup>L. Gentile, C. O. Rossi, U. Olsson, and G. A. Ranieri, "Effect of shear rates on the MLV formation and MLV stability region in the C<sub>12</sub>E<sub>5</sub>/D<sub>2</sub>O system: Rheology and rheo-NMR and rheo-SANS experiments," *Langmuir* **27**, 2088–2092 (2011).
- <sup>26</sup>L. Gentile, K. Mortensen, C. O. Rossi, U. Olsson, and G. A. Ranieri, "Multi-lamellar vesicle formation in a long-chain nonionic surfactant: C<sub>16</sub>E<sub>4</sub>/D<sub>2</sub>O system," *J. Colloid Interface Sci.* **362**, 1–4 (2011).
- <sup>27</sup>L. Gentile, B. F. B. Silva, S. Balog, K. Mortensen, and U. Olsson, "Structural transitions induced by shear flow and temperature variation in a nonionic surfactant/water system," *J. Colloid Interface Sci.* **372**, 32–39 (2012).
- <sup>28</sup>L. Gentile, C. O. Rossi, and U. Olsson, "Rheological and rheo-SALS investigation of the multi-lamellar vesicle formation in the C<sub>12</sub>E<sub>3</sub> system," *J. Colloid Interface Sci.* **367**, 537–539 (2012).
- <sup>29</sup>C.-Y. D. Lu, "Sizes of multilamellar vesicles in shear," *Phys. Rev. Lett.* **109**, 128304 (2012).
- <sup>30</sup>D. Sato, K. Obara, Y. Kawabata, M. Iwahashi, and T. Kato, "Re-entrant lamellar/onion transition with varying temperature under shear flow," *Langmuir* **29**, 121–132 (2013).
- <sup>31</sup>H. Shiba, H. Noguchi, and G. Gompper, "Structure formation of surfactant membranes under shear flow," *J. Chem. Phys.* **139**, 014702 (2013).
- <sup>32</sup>L. Gentile, M. A. Behrens, L. Porcar, P. Butler, N. J. Wagner, and U. Olsson, "Multilamellar vesicle formation from a planar lamellar phase under shear flow," *Langmuir* **30**, 8316–8325 (2014).
- <sup>33</sup>A. G. Zilman and R. Granek, "Undulation instability of lamellar phases under shear: A mechanism for onion formation?," *Eur. Phys. J. E* **11**, 593–608 (1999).
- <sup>34</sup>L. Courbin, J. P. Delville, J. Rouch, and P. Panizza, "Instability of a lamellar phase under shear flow: Formation of multilamellar vesicles," *Phys. Rev. Lett.* **89**, 148305 (2002).
- <sup>35</sup>L. Courbin and P. Panizza, "Shear-induced formation of vesicles in membrane phase: Kinetics and size selection mechanisms, elasticity versus surface tension," *Phys. Rev. E* **69**, 021504 (2004).
- <sup>36</sup>F. Nettesheim, J. Zipfel, P. Lindner, and W. Richtering, "Influence of sodium dodecyl sulfate on structure and rheology of aqueous solutions of the non-ionic surfactant tetraethyleneglycol-monododecyl ether (C<sub>12</sub>E<sub>4</sub>)," *Colloids Surf., A* **183-185**, 563–574 (2001).
- <sup>37</sup>R. Dong, Z. Zhong, and J. Hao, "Self-assembly of onion-like vesicles induced by charge and rheological properties in anionic–nonionic surfactant solutions," *Soft Matter* **8**, 7812–7821 (2012).
- <sup>38</sup>K. Sadakane, H. Seto, H. Endo, and M. Shibayama, "A periodic structure in a mixture of D<sub>2</sub>O/3-methylpyridine/NaBPh<sub>4</sub> induced by solvation effect," *J. Phys. Soc. Jpn.* **76**, 113602 (2007).
- <sup>39</sup>K. Sadakane, A. Onuki, K. Nishida, S. Koizumi, and H. Seto, "Salt induced lamellar phase in the mixture of D<sub>2</sub>O and 3-methylpyridine," *Phys. Rev. Lett.* **103**, 167803 (2009).
- <sup>40</sup>K. Sadakane, N. Iguchi, M. Nagao, H. Endo, Y. Melnichenko, and H. Seto, "2D-ising-like critical behavior in mixtures of water and 3-methylpyridine including antagonistic salt or ionic surfactant," *Soft Matter* **7**, 1334 (2011).
- <sup>41</sup>K. Sadakane, Y. Horikawa, M. Nagao, and H. Seto, "The effect of tetraphenylphosphonium chloride on phase behavior and nanoscale structures in a mixture of D<sub>2</sub>O and 3-methylpyridine," *Chem. Lett.* **41**, 1075 (2012).
- <sup>42</sup>K. Sadakane, M. Nagao, H. Endo, and H. Seto, "Membrane formation by preferential solvation of ions in mixture of water, 3-methylpyridine, and sodium tetraphenylborate," *J. Chem. Phys.* **139**, 234905 (2013).
- <sup>43</sup>K. Sadakane, H. Endo, K. Nishida, and H. Seto, "Lamellar/disorder phase transition in a mixture of water/2,6-dimethylpyridine/antagonistic salt," *J. Solution Chem.* **43**, 1722 (2014).
- <sup>44</sup>A. Onuki, S. Yabunaka, T. Araki, and R. Okamoto, "Structure formation due to antagonistic salts," *Curr. Opin. Coll. Int. Sci.* **22**, 59–64 (2016).
- <sup>45</sup>R. Strey, R. Schomacker, D. Roux, F. Nallet, and U. Olsson, "Dilute lamellar and L<sub>3</sub> phases in the binary water-C<sub>12</sub>E<sub>5</sub> system," *J. Chem. Soc., Faraday Trans.* **86**, 2253–2261 (1990).
- <sup>46</sup>C. B. Douglas and E. W. Kaler, "Phase behavior of aqueous mixtures of hexaethylene glycol monododecyl ether and sodium alkylsulfonates," *Langmuir* **7**, 1097–1102 (1991).
- <sup>47</sup>C. J. Glinka, J. G. Barker, B. Hammouda, S. Krueger, J. J. Moyer, and W. J. Orts, "The 30 m small-angle neutron scattering instruments at the National Institute of Standards and Technology," *J. Appl. Crystallogr.* **31**, 430–445 (1998).
- <sup>48</sup>L. Porcar, D. Pozzo, G. Langenbacher, J. Moyer, and P. D. Butler, "Rheo-small-angle neutron scattering at the National Institute of Standards and

- Technology Center for Neutron Research,” *Rev. Sci. Instrum.* **82**, 083902 (2011).
- <sup>49</sup>S. R. Kline, “Reduction and analysis of SANS and USANS data using IGOR pro,” *J. Appl. Crystallogr.* **39**, 895–900 (2006).
- <sup>50</sup>M. Doucet *et al.*, SasView Version 4.1, Zenodo, <http://doi.org/10.5281/zenodo.438138>.
- <sup>51</sup>N. Rosov, S. Rathgeber, and M. Monkenbusch, “Neutron spin echo spectroscopy at the NIST Center for Neutron Research,” *ACS Symp. Ser.* **739**, 103–116 (2000).
- <sup>52</sup>R. T. Aзуah, L. R. Kneller, Y. Qiu, P. L. W. Tregenna-Piggott, C. M. Brown, J. R. D. Copley, and R. M. Dimeo, “DAVE: A comprehensive software suite for the reduction, visualization, and analysis of low energy neutron spectroscopic data,” *J. Res. Natl. Inst. Stand. Technol.* **114**, 341 (2009).
- <sup>53</sup>F. Nallet, R. Laversanne, and D. Roux, “Modelling x-ray or neutron scattering spectra of lyotropic lamellar phases: Interplay between form and structure factors,” *J. Phys. II* **3**, 487–502 (1993).
- <sup>54</sup>A. Caillé, “Remarques sur la diffusion des rayons X dans les smectiques A,” *C. R. Acad. Sci. Paris, Ser. B* **274**, 891–893 (1972).
- <sup>55</sup>A. G. Zilman and R. Granek, “Undulations and dynamic structure factor of membranes,” *Phys. Rev. Lett.* **77**, 4788–4791 (1996).
- <sup>56</sup>M. Nagao, S. Chawang, and T. Hawa, “Interlayer distance dependence of thickness fluctuations in a swollen lamellar phase,” *Soft Matter* **7**, 6598–6605 (2011).
- <sup>57</sup>B. Farago, M. Monkenbusch, K. D. Goecking, D. Richter, and J. S. Huang, “Dynamics of microemulsions as seen by neutron spin echo,” *Phys. B* **213-214**, 712–717 (1995).
- <sup>58</sup>S. Komura, T. Takeda, Y. Kawabata, S. K. Ghosh, H. Seto, and M. Nagao, “Dynamical fluctuation of the mesoscopic structure in ternary C<sub>12</sub>E<sub>5</sub>-water-*n*-octane amphiphilic system,” *Phys. Rev. E* **63**, 041402 (2001).
- <sup>59</sup>M. Imai, R. Mawatari, K. Nakaya, and S. Komura, “Inter-lamellar interactions modulated by addition of guest components,” *Eur. Phys. J. E* **13**, 391–400 (2004).
- <sup>60</sup>J.-H. Lee, S.-M. Choi, C. Doe, A. Faraone, P. A. Pincus, and S. R. Kline, “Thermal fluctuation and elasticity of lipid vesicles interacting with pore-forming peptides,” *Phys. Rev. Lett.* **105**, 038101 (2010).
- <sup>61</sup>R. Bradbury and M. Nagao, “Effect of charge on the mechanical properties of surfactant bilayers,” *Soft Matter* **12**, 9383–9390 (2016).
- <sup>62</sup>M. C. Watson and F. L. H. Brown, “Interpreting membrane scattering experiments at the mesoscale: The contribution of dissipation within the bilayer,” *Biophys. J.* **98**, L09–L11 (2010).
- <sup>63</sup>U. Seifert and S. A. Langer, “Viscous modes of fluid bilayer membranes,” *Europhys. Lett.* **23**, 71–76 (1993).
- <sup>64</sup>R. Schomaecker and R. Strey, “Effect of ionic surfactants on nonionic bilayers: Bending elasticity of weakly charged membranes,” *J. Phys. Chem.* **98**, 3908–3912 (1994).
- <sup>65</sup>N. Tsapis, R. Ober, and W. Urbach, “Modification of elastic constants by charge addition to a nonionic lamellar phase,” *Langmuir* **16**, 2968–2974 (2000).
- <sup>66</sup>M. Winterhalter and W. Helfrich, “Effect of surface charge on the curvature elasticity of membranes,” *J. Phys. Chem.* **92**, 6865–6867 (1988).
- <sup>67</sup>H. N. W. Lekkerkerker, “Contribution of the electric double layer to the curvature elasticity of charged amphiphilic monolayers,” *Phys. A* **159**, 319–328 (1989).
- <sup>68</sup>M. Winterhalter and W. Helfrich, “Bending elasticity of electrically charged bilayers: Coupled monolayers, neutral surfaces, and balancing stresses,” *J. Phys. Chem.* **96**, 327–330 (1992).
- <sup>69</sup>J. L. Harden, C. Marques, J. F. Joanny, and D. Andelman, “Membrane curvature elasticity in weakly charged lamellar phases,” *Langmuir* **8**, 1170–1175 (1992).
- <sup>70</sup>A. Fogden, J. Daicic, D. J. Mitchell, and B. W. Ninham, “Electrostatic rigidity of charged membranes in systems without added salt,” *Phys. A* **234**, 167–188 (1996).
- <sup>71</sup>Y. W. Kim and W. Sung, “Effects of charge and its fluctuation on membrane undulation and stability,” *Europhys. Lett.* **58**, 147–153 (2002).
- <sup>72</sup>L. M. Bergström, “Bending elasticity of charged surfactant layers: The effect of mixing,” *Langmuir* **22**, 6796–6813 (2006).
- <sup>73</sup>B. Farago and M. Gradzielski, “The effect of the charge density of microemulsion droplets on the bending elasticity of their amphiphilic film,” *J. Chem. Phys.* **114**, 10105–10122 (2001).
- <sup>74</sup>R. de Vries, “Thermal undulations in salt-free charged lamellar phases: Theory versus experiment,” *Phys. Rev. E* **56**, 1879–1886 (1997).
- <sup>75</sup>H. von Berlepsch and R. de Vries, “Weakly charged lamellar bilayer system: Interplay between thermal undulations and electrostatic repulsion,” *Eur. Phys. J. E* **1**, 141–152 (2000).
- <sup>76</sup>N. Awata, K. Minewaki, K. Fukuda, M. Fujii, and T. Kato, “Phase behaviors and light scattering for dilute mixtures of C<sub>12</sub>E<sub>5</sub> and lauric acid,” *Colloids Surf., A* **183-185**, 449–455 (2001).
- <sup>77</sup>D. Roux, C. R. Safinya, and F. Nallet, in *Micelles, Membranes, Microemulsions, and Monolayers*, edited by W. M. Gelbart, A. Ben-Shaul, and D. Roux (Springer Verlag, New York, 1994).
- <sup>78</sup>A. C. Cowley, N. L. Fuller, R. P. Rand, and V. A. Parsegian, “Measurement of repulsive forces between charged phospholipid bilayers,” *Biochemistry* **17**, 3163–3168 (1978).
- <sup>79</sup>D. Roux and C. R. Safinya, “A synchrotron X-ray study of competing undulation and electrostatic interlayer interactions in fluid multimembrane lyotropic phases,” *J. Phys.* **49**, 307–318 (1988).
- <sup>80</sup>F. Nallet, D. Roux, and J. Prost, “Hydrodynamics of lyotropic smectics: A dynamic light scattering study of dilute lamellar phases,” *J. Phys.* **50**, 3147–3165 (1989).
- <sup>81</sup>C. Safinya, D. Roux, G. Smith, S. Sinha, P. Dimon, N. Clark, and A. Bellocq, “Steric interactions in a model multimembrane system: A synchrotron x-ray study,” *Phys. Rev. Lett.* **57**, 2718–2721 (1986).
- <sup>82</sup>G. Bouglet and C. Ligoure, “Polymer-mediated interactions of fluid membranes in a lyotropic lamellar phase: A small angle x-ray and neutron scattering study,” *Eur. Phys. J. B* **9**, 137–147 (1999).
- <sup>83</sup>G. Brotons, M. Dubois, L. Belloni, I. Grillo, T. Narayanan, and T. Zemb, “The role of counterions on the elasticity of highly charged lamellar phases: A small-angle x-ray and neutron-scattering determination,” *J. Chem. Phys.* **123**, 024704 (2005).
- <sup>84</sup>W. Helfrich, “Elastic properties of lipid bilayers: Theory and possible experiments,” *Z. Naturforsch., C: J. Biosci.* **28**, 693–703 (1973).
- <sup>85</sup>T. C. Lubensky, J. Prost, and S. Ramaswamy, “Crumpling and second sound in lyotropic lamellar phases,” *J. Phys.* **51**, 933–943 (1990).
- <sup>86</sup>N. Tsapis, W. Urbach, and R. Ober, “Dramatic rigidification of a peptide-decorated lamellar phase,” *Phys. Rev. E* **63**, 041903 (2001).
- <sup>87</sup>F. Castro-Roman, G. Porte, and C. Ligoure, “Renormalization of Helfrich’s interactions between fluid membranes in a lyotropic lamellar phase by addition of amphiphilic copolymers,” *Phys. Rev. Lett.* **82**, 109–112 (1999).
- <sup>88</sup>L. Porcar, G. G. Warr, W. A. Hamilton, and P. D. Butler, “Shear-induced collapse in a lyotropic lamellar phase,” *Phys. Rev. Lett.* **95**, 078302 (2005).